Extracting Phenological Signals From Multiyear AVHRR NDVI Time Series: Framework for Applying High-Order Annual Splines With Roughness Damping

John F. Hermance, Robert W. Jacob, Bethany A. Bradley, and John F. Mustard

***Abstract*—To better understand how terrestrial vegetative ecosystems respond to climate and/or anthropogenic effects, the scientific community is increasingly interested in developing methods of employing satellite data to track changes in land surface phenology (e.g., timing and rate of green-up, amplitude and duration of growing season, and timing and rate of senescence of plant classes). By increasing the inherent resolution of signal extraction procedures while minimizing the effects of cloud cover and prolonged data gaps, such tools can significantly improve land cover classification and land cover change monitoring on multiple scales. This report describes an intuitive approach for tracking the intra-annual details and interannual variability of multiyear time series, employing a sequence of annual high-order polynomial splines (up to the 14th order), stabilized by minimizing model roughness and weighted to fit the upper data envelope to minimize cloud cover bias. The algorithm is tested using multiyear time series for three very different classes of vegetation—stable agriculture, high elevation montane shrubland, and semiarid grassland with high interannual variability. The results accurately track both short- and long-term land surface phenology and illustrate a robust potential for extracting temporal and spatial detail from a variety of satellite-based multiyear vegetation signals.**

***Index Terms*—Advanced Very High Resolution Radiometer (AVHRR), Fourier analysis, harmonic series, multiyear, normalized difference vegetation index (NDVI), phenology, polynomial fit, signal processing, spline, time series.**

I. Introduction and Overview

A. Motivation for High-Temporal-Resolution Studies of Phenology

In the last few years, the scientific community has shown increasing interest in developing computational tools for extracting subtle signatures of the behavior of vegetation on the Earth's surface through monitoring time series of the normalized difference vegetation index (NDVI) determined from multichannel spectrometers on board Earth-orbiting satellites [1]–[15]. These observations provide a common base of self-consistent long-term time series, from local to global scales. The analysis of such data provides a significant insight into the response of vegetation to short- and long-term environmental forcing effects, both natural and anthropogenic. Since different plant species tend to respond differently to fluctuations of environmental factors, their phenology can be used on a site-by-site (i.e., pixel-by-pixel) basis to identify, or discriminate among, particular land cover types and monitor their response to typical climate and weather conditions, as well as their response to anomalous conditions of extreme drought, storms, and wildfire [16]–[18]. In other words, the nature of interannual (i.e., year-to-year) fluctuations in intra-annual (i.e., seasonal) variations may provide important information for identifying and discriminating among vegetation communities [19]. The signature vegetation behaviors—the phenology—of specific sites over multiple years, with appropriate validation can then be used to formally classify patterns of land cover usage and, consequently, to better monitor short- and long-term land cover changes on local, regional, and global scales [19]. Clearly, the more accurately one can track subtle variations in the timing and amplitude of photosynthetic activity at a site, the more effective will be the techniques for identification of, and discrimination among, vegetation communities.

To effectively track high-order interannual variations in NDVI time series, this report describes a new simple but robust data-adaptive weighted recursive least squares (LS) modeling procedure using high-order annual splines for characterizing the detailed intra-annual and interannual behaviors of representative members of vegetation classes for multiyear time series. Although, in principle, local functionals such as Gaussian forms [7], [8], logistic forms [10], [14], or wavelets [20] could be used to model phenology over subannual intervals, we elect to employ a sequence of annual high-order splines as the basis functions for our interannual model. Each class of functionals has its particular advantages, but for this application, we favor splines because of the ease of coding and their intrinsic adaptability to a variety of intra-annual fluctuations (e.g., multiple green-up cycles). In addition, it is relatively easy to enforce interannual continuity of the functional behaviors. At the join between annual subintervals (i.e., the "knots" of the spline), we explicitly enforce the condition that the value of the spline functionals and their first and second derivatives are continuous.

One must recognize, of course, and compensate for the intrinsic instability of high-order polynomials when fitting noisy data, particularly when there are significant intervals of missing values [such as the loss of data for some months in 1994 due to the failure of the Advanced Very High Resolution

Manuscript received June 12, 2006; revised March 21, 2007.

The authors are with the Department of Geological Sciences, Brown University, Providence, RI 02912 USA (e-mail: john_hermance@brown.edu).

Digital Object Identifier 10.1109/TGRS.2007.903044

Radiometer (AVHRR) instrument on board NOAA-11]. To regularize the stability of the resultant functionals, we use the three key elements of a procedure that was originally developed to model the average annual variation of phenology [21]. Here, the method is extended to model interannual variations in phenology as well. First, we begin by computing a robust initial starting model—a baseline average annual representation that will be recursively refined—as well as provide preliminary estimates of data values during data gaps. Next, we regularize our optimization procedure by minimizing model roughness (which is to say we apply the "roughness damping" procedure of Hermance [21] over specified time intervals). Finally, due to the tendency for cloud cover and other atmospheric obscurations to downward bias NDVI values, our procedure is asymmetrically biased to preferentially fit the upper envelope of observed data values. We illustrate the adaptability of our algorithm by applying it to representative multiyear time series of standard weekly and biweekly 1×1 km composites of the AVHRR NDVI from the Great Basin of Western North America. The following three classes of vegetation have been selected, distinctly demonstrating different interannual variation patterns: 1) stable agriculture; 2) high elevation montane shrubland; and 3) semiarid grassland. The focus of our discussion here is to describe the algorithm. In a related report, Bradley *et al.* [19] give examples of using this algorithm to characterize the phenology of a broader variety of land cover classes in the Great Basin, with a specific application to land cover classification and land cover change issues.

TABLE I
REPRESENTATIVE ATTRIBUTES OF PLANT PHENOLOGY TO BE IDENTIFIED FROM NDVI DATA (cf. [23])

1. Time for the onset of green-up;
2. Maximum rate of green-up;
3. Time of maximum NDVI;
4. Amplitude of maximum NDVI;
5. Time for the onset of senescence;
6. Details of senescence;
7. Maximum rate of senescence;
8. Time of termination of senescence and beginning of dormancy;
9. Inter-seasonal range of NDVI;
10. Time-integrated NDVI (as a measure of net primary productivity).

II. PAST WORK ON EXTRACTING THE PHENOLOGICAL SIGNAL FROM NDVI DATA

A. Determining Average Seasonal Patterns

1) Applications of Classical Harmonic Analysis: Among the first "phenological" applications of satellite data in North America was that of Rouse *et al.* [22], who constructed a series of synoptic maps to monitor the progression of seasonal vegetation patterns across the rangelands of the central U.S. Great Plains. Reed *et al.* [23] emphasized the importance of using remotely sensed satellite data to parameterize phenological "events" on an ecosystem scale—the aggregated monitored response of vegetation over a subarea to the annual cycle of weather patterns, soil moisture, and temperature. Such information might provide signature information on land cover types, plant conditions, and land cover changes. To do so, they proposed a set of observable metrics, such as the time of onset of green-up and senescence, maximum rates of green-up and senescence, the time and amplitude of maximum NDVI, of which representative members are listed in Table I. In this report, we use these metrics as target parameters to be identified by our new algorithm and smoothly tracked on seasonal and interannual bases. In a related paper, Bradley *et al.* [19] document how selected members of these parameters can actually be extracted from the algorithm and applied to land cover classification and changes.

Because phenologies typically have strong seasonal cycles, modeling the observations with the Fourier or harmonic series has become one of the principal methods of analysis. Moody and Johnson [3] present a comprehensive review of the theory and the literature of what Jonsson and Eklundh [7], [8] refer to as the "classical" harmonic method applied to NDVI data prior to the early 2000s. Menenti *et al.* [24], Sellers *et al.* [25], Olsson and Eklundh [26], and Andres *et al.* [27] were among the first to use classical spectral methods to identify some of the key phenological elements in NDVI time series. This was followed by the work of Azzali and Menenti [1], Roerink *et al.* [2], Jakubauskas *et al.* [4]–[6], and Moody and Johnson [3]. Geerken *et al.* [13] used a synthesized low-pass-filtered time series from a band-limited discrete Fourier transform (DFT) of NDVI data in a lagged cross correlation analysis to classify native rangelands in the Middle East. As an alternative to the latter approach, Evans and Geerken [28] developed a DFT-based classification algorithm using a metric based on the similarity of the frequency-domain phase and scaled-amplitude components of the annual harmonics of an unknown test pixel to a reference pixel from a known class. They argue that the algorithm is very efficient, computationally, in classifying rangeland vegetation by dominant shrub type in the Middle East.

Thus, classical Fourier methods have become a standard tool for analyzing annual data, particularly those comprised of monthly averaged samples from multiple years. However, underlying the application of classical harmonic methods is the implicit expectation that the observed data are sampled at uniform intervals of time, which often poses a problem for typical NDVI data, particularly when there are extensive data gaps. Moreover, one needs to assume that the "harmonics," i.e., the frequencies employed for the trigonometric terms, are truly harmonics of the record length, and in some cases one might need to assume, if one is constructing an average annual model from a multiyear data set, that the sampling occurs at the same relative time each year. It is possible, however, to use a more general approach to harmonic analysis to relieve these restrictions [7], [25]—a procedure that Hermance [21] refers to as "nonclassical" harmonic or Fourier analysis.

2) Nonclassical Harmonic Analysis: A straightforward though computationally more intensive extension of the classical Fourier method better adapts to the practical realities of NDVI data quality, such as nonuniform time samples, sudden anomalous decreases in data values due to cloud and ground cover, extended data gaps, and long-term trends: nonclassical harmonic analysis [7], [21], [25]. This procedure solves the LS minimization relation for a predicted model or data value d_{pred} at arbitrary times t_i using an optimal set of nonorthogonal basis functions that are user-specified according to the intrinsic nature of the observations being modeled. For analyzing NDVI data, it has been useful [7], [8], [21] to employ a composite of annual harmonics and a low-order polynomial trend of the form

$$d_{\mathrm{pred}}(t_i) = \sum_{k=0}^{L} c_k t_i^k + \sum_{j=1}^{M} \left(a_j \cos\left(\frac{2\pi j}{T} t_i\right) + b_j \sin\left(\frac{2\pi j}{T} t_i\right)\right) \tag{1}$$

where L is the order of the polynomial trend (which is typically order 1 or 2), T is the characteristic fundamental period (which is typically one year), and M is the order of the harmonic series. The consequence for the more flexible and practical choice of nonorthogonal basis functions is that one has to solve the complete matrix form of the LS penalty relation, rather than the simple algebraic forms associated with the classical Fourier analysis (or the DFT and fast Fourier transform). However, the additional computational overhead is warranted in some cases. Hermance [21] concludes that the temporal resolution of these techniques is significantly improved if, along with a weighted minimization of the sum-of-the-squared-data residuals so as to track the upper envelope of observed data, one also enforces an expectation of minimum model roughness to dampen spurious oscillations in predicted values. Upon doing so, one can significantly increase the order of the harmonic series, resulting in annual models that have resolutions that are consistent with the results from applying special transcendental forms such as asymmetric Gaussian and logistic (sigmoidal) functions discussed in the following.

B. Resolving Short-Term Intra-Annual and Interannual Variations

1) Alternatives to Harmonic Series: There is an increasing interest in the community in using refined mathematical models to characterize the rapid transient response of certain specific vegetation classes to typical annual forcing terms, as well as to track the intrinsic year-to-year variability of photosynthetic activity due to local and regional climatic anomalies [7], [8], [10], [11], [14], [15], [19], [20]. Wagenseil and Samimi [29] note that classical Fourier analysis methods are limited in this regard, although Lunetta *et al.* [30] applied a DFT method to five years (2000–2004) of NDVI data to detect interannual changes in land cover in the east-central U.S.

However, to capture the most dynamic evidence of land cover change, workers have considered alternatives to harmonic series, since the higher order terms that are needed to track shorter period fluctuations often generate spurious parasitic oscillations in the modeled NDVI time series [11].

One approach is to use local functional forms or aperiodic transients to represent seasonal fluctuations in NDVI values on annual or subannual time scales. Historically, the most common functional used by numerical analysts for generating phenomenological models for a variety of applications is a simple power series of order M (cf. [31] and [32]). With simple coding, such forms are adaptable to a variety of implicit and explicit conditions on the functional's attributes.

However, the tendency for polynomial series to be intrinsically unstable for less than ideal cases is legendary [31]. Lancaster and Salkauskas [32], among others, show examples that underscore the tendency of such functionals to generate spurious artifacts, particularly when data are not well conditioned or when there are significant data gaps, as is often the case with NDVI values. Without question, one needs to be wary in using simple polynomial series to represent actual data, and in the last few years, such concerns have led to the development of several refinements described in the following.

2) Wavelet Analysis: Li and Kafatos [20] apply wavelet decomposition to analyze the effect of El Niño on interannual NDVI anomalies in the U.S. Sakar and Kafatos [12] used wavelets to study the impact of monsoon precipitation on the interannual variability of vegetation over the Indian subcontinent. This type of analysis was used by Sarkar *et al.* [33] to demonstrate what they interpret to be evidence that particular land covers are responsible for local increases in precipitation in Southeast Asia.

3) Asymmetric Gaussian Functions: Jonsson and Eklundh [7], [8] describe a method for extracting seasonality information from NDVI data using nonlinear LS fits of piecewise-defined asymmetric Gaussian functions to the time series. By arranging a sequence of these functionals that were defined and appropriately tapered over adjacent time intervals, they build a global function that describes the fluctuations in observed NDVI values. Incidentally, the original observed data do not have to be sampled at uniform rates.

4) Asymmetric Logistic or Sigmoidal Functions: As an alternative, Zhang *et al.* [10], Beck *et al.* [14], and Fisher *et al.* [15] use double logistic or sigmoidal functions as their local basis functions. Although not so universally known as Gaussian functions, the logistic or sigmoidal functions are basically composite transcendental functions that have evolved from solutions of certain classes of differential equations and are commonly used in modeling neural networks and fuzzy logic applications (such as in MatLab packages). These functionals, as was the case for the asymmetric Gaussian functions, can also be applied to data that are not uniformly sampled in time.

5) General Comments on Local Functional Forms: In assessing which class of functionals to use, one's concern would probably not be with intrinsic accuracy, since all can apparently, with experience, be tuned to an approximately the same degree of "fit." Rather, one would likely be concerned with how flexibly the various functionals can be adjusted to fit the requisite attributes of specific applications. Some forms are best applied to seasonal data that have single simple maxima during the

summer and single simple minima during the dormant seasons (as opposed to those time series that exhibit several peaks or troughs in photosynthetic activity during an annual cycle). Other forms have been used primarily for characterizing intra-annual fluctuations (e.g., multiple green-up cycles in a single year). Here, we are concerned with implementing the use of local functional forms in tracking a variety of intra-annual and interannual phenological behaviors in multiyear time series—some phenologies are consistently repetitive in patterns from year to year; others show substantial variability in annual patterns, depending on local natural or anthropogenic external forcing. Can one class of functionals be adapted to fit such a variety of phenologies?

C. Requirements for a High-Resolution Signal Extraction Algorithm

In this paper, to better identify and discriminate among vegetation communities, our primary concern is with increasing the time and amplitude resolution with which we can track subtle differences in the year-to-year behaviors of seasonal phenology as closely as possible. This is particularly true for the type of transient amplified response that certain land cover types—e.g., semiarid annual grasslands—exhibit in response to anomalous episodes of increased precipitation [19]. We need to capture not only the essence of persistent seasonal cycles in the data, as is done with average annual harmonic models, but also aperiodic transient signals that have relatively short characteristic times. In addition, we need to minimize the effects of clouds, other atmospheric obscurations, and anomalous land cover, e.g., from ephemeral water bodies and snow cover, while maintaining a stable behavior in the vicinity of substantial data gaps. Finally, we would like an algorithm whereby one size fits all, i.e., an algorithm that is computationally robust (which means that it is computationally stable for a variety of data classes) yet computationally adaptive (which means that the procedure can adapt to closely tracking a variety of diverse vegetation community responses with a minimum of hands-on fine-tuning of parameters).

III. Implementing a New Signal Extraction Algorithm

A. Modeling Interannual Fluctuations With High-Order Splines

To meet the above objectives, we elect to employ high-order splines as the basis functions for our interannual model. Splines are essentially refined versions of the high-order polynomial form described above and are defined for this application in the following way. If a multiyear time series of L years period of record is to be analyzed, then we divide the period of record into L annual subintervals. Here, for example, for a time base that runs within $1995.00 \leq t < 2002.00$ (where the decimal values denote the respective time in calendar years of the center time of a composite NDVI sample), we have $L = 7$ subintervals or years. In this case, the subscript of the kth subinterval runs from $k = 1$ for the first year through $k = k_{\max} = L = 7$ for the final year. Within each of the $k = 1$ to L subintervals, we define a local Mth-order polynomial as follows:

$$d^{(k)}_{\mathrm{pred}_i} = \sum_{j=0}^{M} a_{kj} t^j_{ki} \tag{2}$$

where k is the index of the kth yearly subinterval, i is the index of the predicted data at the time sample t_{ki}, which is raised to the jth integer power during the summation on the right-hand side of the relation, and a_{kj} is the coefficient of the jth member of the local power series that is piecewise defined for the kth subinterval. Note that the subscript k for the time term t^j_{ki} is used to account for the transformation of the global time base in calendar years (scaled, for example, from 1995.00 to 2001.99) to a local time base defined for computational reasons from -0.50 to $+0.50$ for individual years. Although this complicates the bookkeeping in the programming somewhat, it is an effective way to deal with issues of computer roundoff errors and leads to a significant improvement in the precision and, ultimately, the stability of the computation.

At the join between annual subintervals (the joins are usually referred to as the "knots" of the spline), we explicitly enforce the condition that the value of the spline functionals and their first and second derivatives are continuous. This differs somewhat from conventional spline interpolation (e.g., Esch [34]) in that, for the latter, all derivatives up to and including order $M-1$ are continuous across the knots. Such a stringent set of conditions is relaxed in our case, since we are employing the auxiliary condition of minimum model roughness on the LS solution, which implicitly constrains the derivatives and suppresses instabilities [21].

B. Construction of a Robust Initial Starting Model

There is a significant advantage to initializing our procedure by computing an average annual model using the general nonorthogonal harmonic series with the nonlinear trend given by (1). This initial model serves a twofold purpose. First, the average annual model provides an estimate of "missing" (or rejected) data, particularly during extended data gaps, which tends to constrain the behavior of the next stage models, hence, reducing tendencies toward local instabilities and providing a robust starting model. Second, residuals between the observed data and predicted values from the average annual model provide the basis for assigning weights based on initial model misfit parameters when computing refined models, as discussed in the following.

C. Procedures for "Tuning" the Model Response

1) Minimizing Roughness: As a complement to the objective of generating a function that "fits" our observed data to some defined level of precision, we expect our model not to exhibit spurious oscillations and to smoothly track the data without significant overshooting or undershooting. In other words, we expect minimum roughness in our model. To this end, we define, for computational convenience, the total local model "roughness" as the sum of the squared values of the

second derivative of the model function over a predefined interval (or intervals) of interest (for details, see [21]). The actual time interval over which minimum roughness is applied is based on a preliminary inspection of the data, experience regarding the expected outcome, and one or more preliminary pilot computations.

For a general function $f(t)$, over the local time interval having indices i_{start} to i_{end}, a measure of model roughness can be expressed numerically as

$$\text{Roughness} = \sum_{i_{\text{start}}}^{i_{\text{end}}} \left[\partial^2 d_{\text{pred}}(t_i)/\partial t^2\right]^2. \tag{3}$$

Minimizing this parameter with regard to the respective model parameters is invoked as a complementary minimization criterion when constructing our LS operation [21].

2) Asymmetric Weighting to Fit the Upper Envelope of Observations: Residuals between the original observed NDVI values and those "predicted" by an initial starting model are computed for the ith time sample as

$$\Delta d(i) = d_{\text{obs}}(i) - d_{\text{pred}}(i) \tag{4}$$

where $d_{\text{obs}}(i)$ is the observed data value for the ith time sample, and $d_{\text{pred}}(i)$ is the data value predicted by the (prior) model, respectively. We assign a Gaussian-type weight of the form

$$\text{Weight} \propto \exp\Big(\text{sign}\left(|\Delta d|/w\right)^2\Big) \tag{5}$$

where sign is an operator that has a value of -1 if Δd is negative or $+1$ if Δd is positive. The parameter w defines the "width" of the Gaussian operator; a typical value might be $w = 0.01$ NDVI units. Generally, each data value is assigned a weighting factor given by

$$\text{Weight}(i) = \text{Weight}_{\text{Missing data}} \exp(\text{sign}\left(|\Delta d|/w\right)^p) \tag{6}$$

where the exponential expression is a generalized version of the form given above, such that p need not necessarily be an integer value. We typically begin with a value of $p = 2$ in (6) (as it would be for a Gaussian), but we may adjust its value, depending on the outcome from several pilot model runs. The leading coefficient $\text{Weight}_{\text{Missing data}}$ allows for weighting the values of actual observed data differently from the estimated values of missing data (i.e., those values inferred from a prior trial model).

D. Implementing the Procedure

1) Base Average Annual Model: As the initial step in our procedure, we construct the average annual phenological behavior for a site from multiyear time series using a nonorthogonal harmonic series with a nonlinear trend. If a more refined average annual model is required, we have the option of applying roughness damping during data gaps and during intervals when one would expect minimal fluctuations in NDVI values, such as during the dormant winter season. Finally, due to cloud cover and other atmospheric obscurations, we have the option to asymmetrically bias the procedure to preferentially fit the upper envelope of observed data values (cf. [7], [21], and [25]).

2) Interannual High-Order Spline Model: As we proceed with computing the interannual model—a representation of the seasonal and year-to-year fluctuation of vegetation—we apply a multistage recursive weighted LS fit to the data by using a set of annual higher order splines with roughness damping during intervals when fluctuations in photosynthetic activity are expected to be minimal (in our case, local winter). To bias the predicted model values toward local maxima, the algorithm uses asymmetric weighting of the residuals such that high data values are up-weighted and low data values are down-weighted, which tends to detect the upper envelope of observed data values. For some data types—those with regular phenologies and slow single cycle intra-annual variability—lower order computationally efficient splines are quite adequate for representing the data. For other data types—those with greater interannual variability, perhaps abrupt green-up, and senescence and/or several growth cycles in a season, or sudden conversions of land cover type—higher order splines may be required, with a concomitant penalty in computer time. We typically use from eighth- to 14th-order annual splines, preferring the larger orders for the final stage of analysis. Whereby a 14th-order polynomial may be intrinsically unstable for some NDVI data, particularly when there are significant data gaps, the splined version of this application is quite stable due to three principal aspects of our procedure: 1) the explicit continuity conditions on the functional values and their first and second derivatives across "knots" (i.e., across contiguous years); 2) filling data gaps with values predicted by an initial model; and 3) selectively invoking the expectation of minimum model roughness.

IV. Application of the Procedure

A. Study Area

We illustrate these techniques using standard weekly and biweekly AVHRR NDVI data composites for 1×1 km pixels from the NOAA polar-orbiting satellites for the Great Basin in western North America (Fig. 1). NDVI data for the U.S. are a standard product of the U.S. Geological Survey's National Center for Earth Observation and Science (EROS) that was reduced from multiband spectrometers on board NOAA-11, NOAA-14, and NOAA-16 satellites (see EROS [35], which is an update of [36]–[39]). The NDVI data that are presented here have been rescaled from the byte data range (0–200), as delivered by EROS, to NDVI-computed values ranging from -1.0 to 1.0. Since values on the order of 0 or less represent clouds, snow, water, and other nonvegetative surfaces, to regularize our fitting procedure, we have the option of setting NDVI values less than 0 to be equal to 0, or treating values on the order of 0 or less as missing values. For the examples that are shown later in this paper, we opt for the former.

The time series that we have selected for our examples are from a subset of sites (or pixels) for the much larger region of the Great Basin studied by Bradley *et al.* [19]. We find it useful to compare the results of our interannual modeling to the average annual models of Hermance [21] and use data from the

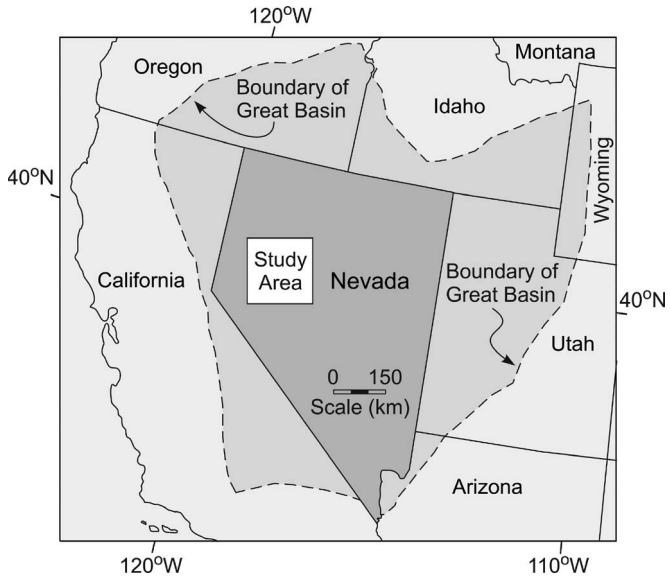

Fig. 1. Location map for our study area in west-central Nevada, along with the names of adjacent states. Also indicated is the boundary of the Great Basin.

same local 150 × 150 km study area in west-central Nevada, as shown in Fig. 1.

The local study area provides a microcosm of a broad range of vegetation classes: from irrigated agriculture with peak annual NDVI values of up to 0.7 to nonvegetated playas (alkali salt flats) with typical annual NDVI values of 0.07.

B. Representative Vegetation Classes Used in This Study

A primary objective of this report is to demonstrate the response of the interannual modeling algorithm to diverse classes of vegetation phenology. We therefore apply our algorithm to a set of time series that represents each of the three classes of vegetation shown in Fig. 2, respectively: stable agricultural areas [panel (a)]; high elevation montane shrublands [panel (b)]; and semiarid grasslands [cheatgrass, panel (c)].

1) Stable Agriculture Data: Panel (a) in Fig. 2 shows a representative seven-year time series of NDVI values from an actively irrigated agricultural site typical of data from a number of sites in the Lovelock and Fallon, NV, agricultural districts. In selecting a representative "stable agriculture site," data from all 1 × 1 km sites (pixels) in the 150 × 150 km study area (a total of 22 500 sites or pixels) were statistically screened for maximum NDVI values and minimum variation within respective growing seasons and between years, leading to time series from 20 candidate sites (or "pixels"). Of these, we then randomly selected a representative member that has a time series of consistently high NDVI values over extended intervals in the summers of all years. Due to active cultivation and irrigation of this class of sites, this member time series demonstrates a very consistent interannual pattern in the behavior of seasonal phenology [Fig. 2, panel (a)].

2) Montane Shrubland Data: The middle panel [panel (b)] in Fig. 2 shows a representative time series for montane shrubland data randomly selected from a rectangular block of 44 contiguous sites (pixels) in the Desatoya Mountains, a relatively high elevation (typically ≥ 2500 m) mountain range in our study area. Of the 44 time series, data from this site were selected from among those having the highest NDVI values, as well as the largest maximum-to-minimum seasonal variations. The large amplitude fluctuation of these high elevation data is, of course, associated with persistent close-to-zero minima due to a very strong imprint of snow cover in winter. What our analysis will show is that our procedure is quite adept at detecting the timing of snow-cover meltdown for these data in spring time. This member time series [Fig. 2, panel (b)] shows a dominant annual periodicity, but since the montane shrubland sites are subject to natural climate variations, there is more interannual variability in the phasing and amplitude of phenology at the montane site than for the time series from the artificially controlled stable agriculture site shown in panel (a).

3) Cheatgrass—An Invasive Semiarid Grassland Species: Fig. 2(c) shows the characteristic time series for cheatgrass (*Bromus tectorum*), an invasive annual grassland species that tends to replace more productive native semiarid grass species. This sample time series is taken from one of 12 contiguous cheatgrass sites identified in the field by Bradley and Mustard [40] and referred to in their paper as Type Area A. Here, for purposes of assessing our algorithm, we have selected a time series based on the extreme response of the data to the anomalous interval of precipitation experienced in the Great Basin in 1998. Bradley and Mustard [40] and Bradley *et al.* [19] have argued that the singular amplified response of cheatgrass to rainfall (distinct from native shrub/bunch grass in the Great Basin) might serve as a diagnostic tool in classifying land cover. A principal reason for developing the present algorithm was to better characterize the unique signature of vegetation communities with strong interannual variability such as these. Clearly, the invasive grassland data in Fig. 2(c), show a much higher degree of interannual variability in phasing and relative amplitude of NDVI values than either the stable agriculture data in panel (a) or the montane shrubland data in panel (b) of this figure.

C. Illustrating the Steps of the Procedure: Using Cheatgrass Data

The panels in Fig. 3 illustrate the results from each step of the procedure applied to the cheatgrass time series in Fig. 2(c). For this example, we have employed four steps beginning with an initial average annual harmonic model as described by Hermance [21] and finishing with a two-stage recursion that employs the interannual spline model.

Step 1) Preliminary LS "Fit" of the Nonclassical Harmonic/Polynomial Composite Function: Following the procedure of Hermance [21], we first compute a simple average annual model with the results shown in of Fig. 3(a). This "initial" average annual harmonic model fit to the observed data employs simple LS without weights and, here, without any implicit smoothing. Currently, we employ the composite harmonic series in (1), consisting of a low-order multiyear polynomial and six cosine and six sine coefficients that have fundamental periods of $T = 12$, 6, 4, 3, 2.4, and 2.0 months. The underlying polynomial is a simple interannual fourth-order polynomial for the complete seven-year period of record.

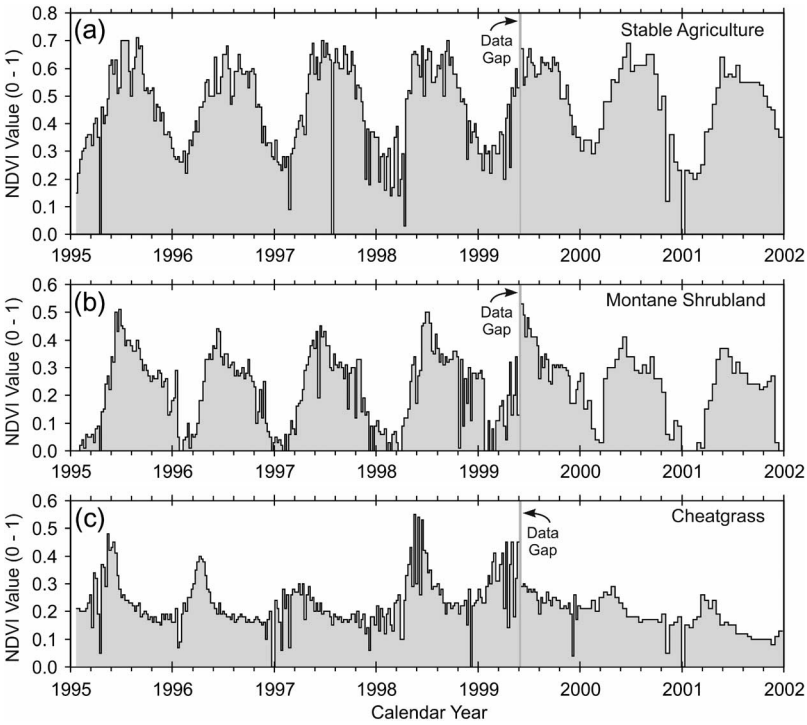

Fig. 2. Original NDVI time series from three classes of vegetation types. (a) Stable agriculture. (b) Montane shrubland. (c) Invasive semiarid annual grasses (cheatgrass). The vertical gray band at ≅1999.4 years (which is actually from the one-week data composite centered at 1999.414) denotes an inferred data gap associated with what is observed as a ubiquitous anomalously high NDVI data value for this interval throughout our Basin and Range database.

The latter is consistent with the second-order polynomial employed by Jonsson and Eklundh [7], [8] since the latter authors are accounting for the trend of a three-year time series, whereas we are accounting for the trend of a seven-year time series. For purposes of illustration, in this example, we do not apply an expectation of minimum roughness for the model. This is for the purpose of illustrating the drawback of using a simple harmonic series of such a large order in which the model tends to have high-order oscillations that, as shown for the early springtime in Fig. 3(a), may be unrealistic. Such instabilities may be of even graver concern during extended data gaps, but as discussed by Hermance [21] and as will described later in this paper, model roughness damping can compensate for such effects.

Step 2) Refined Average Annual Model—Updating the Harmonic/Polynomial Composite Function: Fig. 3(b), shows the second step in our procedure, which is to fit a refined average annual harmonic model to the observed data. This step employs a nonclassical Fourier series [as in (1)], but with the addition of model roughness damping and asymmetrically weighting the data observations for the model to track the upper data envelope. We again use a sixth-order annual harmonic series superimposed on a fourth-order polynomial. Close inspection of Fig. 2(b), will show that applying an expectation of minimum roughness on the synthesized time series has tended to suppress some of the mild oscillatory instabilities that are associated with the model from the initial stage shown in panel (a). In production runs, to optimize computation time, we recommend applying minimum roughness to the model at the earliest stage of the procedure to suppress such spurious effects from the outset.

In comparing the results in panels (a) and (b), note that the simple average annual harmonic model [panel (a)] captures the mean behavior of annual fluctuations (including data dropouts) over all years, whereas the refined average annual model [panel (b)] captures the mean upper data envelope of the annual fluctuations over all years. Both the simple and the refined average annual models account for the long-term trend in the observed data. Although for many applications an average annual model [e.g., panel (b)] may be the end product in its own right (see the review by Hermance [21]), in our procedure, it serves as a starting model for a more refined interannual analysis.

Step 3) First-Stage Interannual Spline Model: Fig. 3(c), shows the first-stage output model using high-order interannual spline functionals as in (2). The first recursion in this example employs seven annual piecewise-defined eighth-order splines for a total of 63 model parameters (counting the zeroth-order term in each spline) for the complete seven-year times series. We also employ interannual roughness damping and upper data envelope tracking. [For multiple recursions, one might opt, as we have done here, to begin with a lower order annual spline to initially ensure stability, moving on to higher order splines in the following recursion(s).] For this preliminary stage, we have also opted not to attempt to fit the extreme highest observed NDVI values. Comparing the observed data and the model results for the average annual model in Fig. 3(b), against the observed data and the model results for the first-stage interannual spline model in Fig. 3(c), shows that, for this class of vegetation, the amplitude and timing of maximum NDVI, as well as the annual timing of the onset of green-up, differ significantly from year to year. The interannual

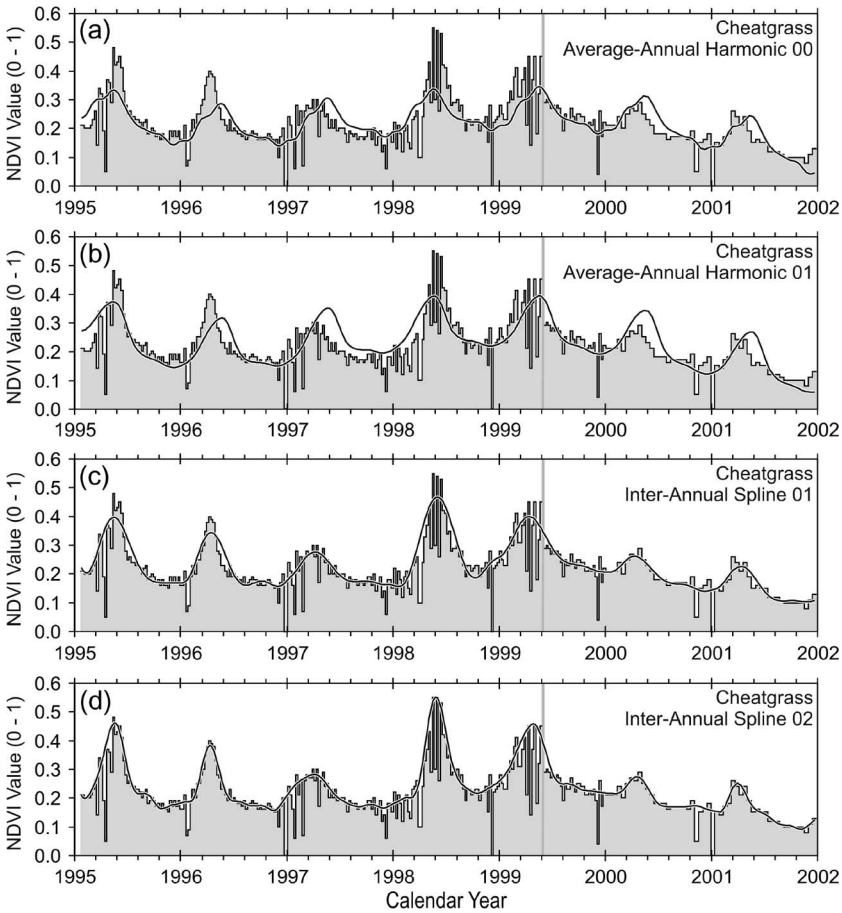

Fig. 3. Illustrative results from each step in the procedure applied to the cheatgrass time series in Fig. 2(c). (a) Step 1: Simple annual harmonic starting model. (b) Step 2: Roughness damped average annual harmonic model weighted to track the upper data envelope. (c) Step 3: Preliminary eighth-order interannual spline model with weak upper-envelope weighting. (d) Step 4: Fourteenth-order interannual spline model with stronger upper-data envelope weighting.

model in panel (c) fits the inferred phenology of each individual year significantly better than the average annual model shown in panel (b). Thus, even a single-stage calculation of the interannual model can provide a significant improvement in tracking interannual variability. However, for this example, this year-to-year variation in phenology is better tracked through refining the model parameters using a second-stage recursion, as discussed in the following section.

Step 4) Refined Interannual Model—Application of High-Order Annual Splines: Using asymmetric weights based on the residuals between the relatively stable fit of the first interannual recursion [panel (c)] and the observed data, we next (in Step 4) go through a second recursion using 14th-order interannual splines, for a total of 105 model parameters (counting the zeroth-order term in each spline) for the complete seven-year times series. In addition, we use somewhat stronger upper-data envelope weighting than that used in Step 3, leading to the fit in Fig. 3(d). A comparison between panels (d) and (c) demonstrates a significant and systematic improvement in the fit between the first and the second recursion of the interannual spline model. For example, the maximum seasonal values in 1995, 1996, 1998, and 1999 are better represented by the second recursion in panel (d). Moreover, employing a higher order spline in Step 4 better tracks the overall photosynthetic cycle in 1995, 1996, and 1998.

Although during testing we have extended our procedure up to five recursions, the improvement in the model usually does not warrant the added computational effort beyond two or three recursions, and the results are not shown here. In fact, for some applications, the analyst might even favor the computational efficiency of using only one carefully "tuned" recursion for the interannual spline. However, if one requires the optimal resolution of temporal fine structure in the phenology, we recommend two, possibly three, recursions of the interannual spline functions.

D. Comparing Results for the Three Vegetation Classes

Figs. 4 and 5 show the results of applying our algorithm to all three classes of vegetation types. To test its "one-size-fits-all" ability, the same set of model control parameters (i.e., the same sequence of culling criteria, assigned model orders, damping functions, asymmetric data weights, number of recursions, etc.) is applied to all three examples. The specific model control parameters were assigned, following several "pilot" runs to simultaneously optimize the fit to all three vegetation classes, and differ from those used for Fig. 3, which had the objective of tracking the upper data envelope as closely as possible for a particular class of vegetation. As shown by Roerink *et al.* [2], a common concern of applying such data-specific algorithms

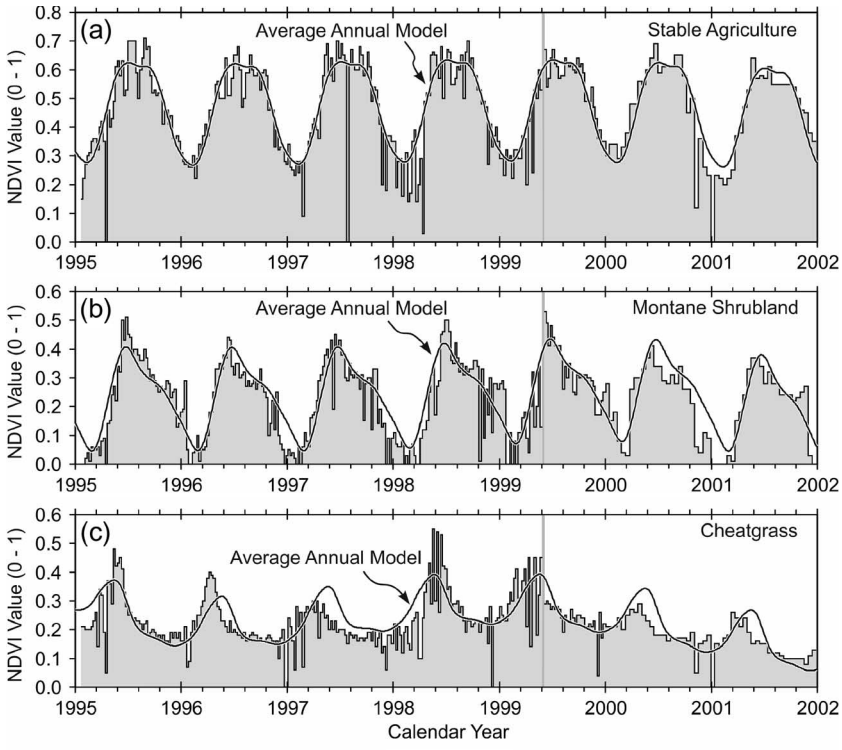

Fig. 4. Average annual variation models for the three classes of vegetation types. All models were computed using the same control parameters (weighting coefficients, roughness damping, etc.).

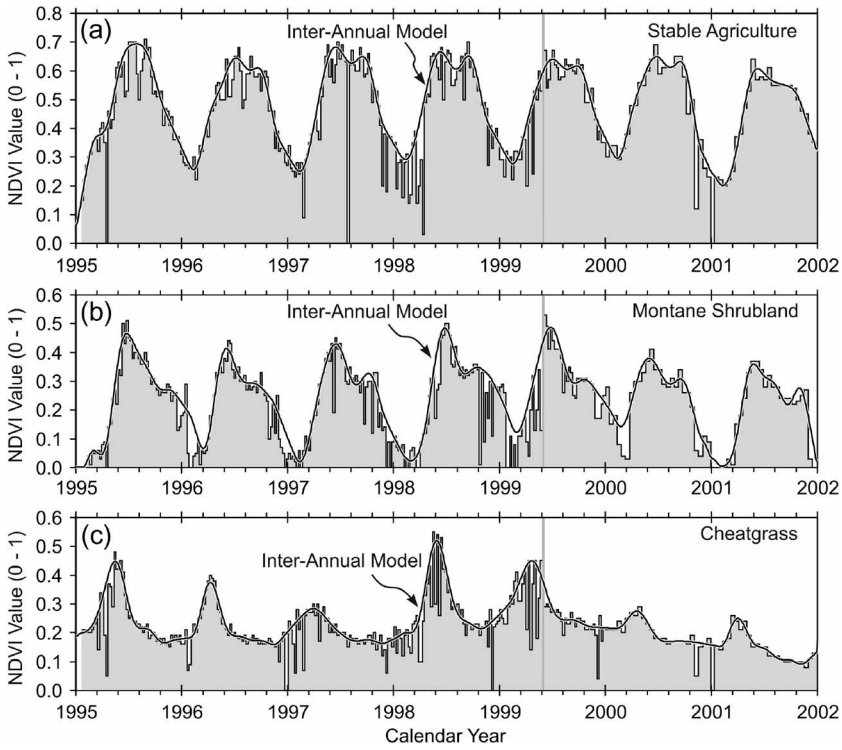

Fig. 5. Interannual model fits for the three classes of vegetation. All models were computed using common asymmetric weighting coefficients and roughness damping control parameters.

(in their case, an annual Fourier harmonic analysis) is that, from a mathematical viewpoint, there is presently no objective basis (such as statistical tests of significance) for determining the control parameters. As Roerink *et al.* [2] concluded, among others, here, the success of a data fit is based on experience and one's *a priori* expectations for what comprises an adequate "fit" to the data. In such applications, model control parameters are set at appropriate values after running several combinations

TABLE II
SUMMARY STATISTICS OF RESIDUALS FROM FINAL INTERANNUAL SPLINE MODEL MISFIT

Statistical parameter	Stable Agriculture	Montane Shrubland	Cheatgrass
Total # of Data:	310	310	310
# positive Δd :	122	110	128
# negative Δd :	188	200	182
Simple statistics			
Global* *sd* all Δd :	0.080	0.066	0.059
sd positive Δd :	0.026	0.028	0.020
sd negative Δd :	0.100	0.080	0.076
Weighted statistics			
Global* *sd* all Δd :	0.032	0.034	0.024
sd positive Δd :	0.028	0.033	0.022
sd negative Δd :	0.035	0.035	0.026

*Standard deviation (*sd*) of all model misfits Δd for all samples in the respective time series.

on representative data sets. Thus, the initial stage of any areal survey, regardless of scale, should involve a sequence of model runs using a set of extreme examples of time series that embody the complete diversity of phenological responses that one expects to encounter in a particular study.

To be concise, Figs. 4 and 5 do not reproduce the results of all four stages of the analysis for the three vegetation classes, as we did for the cheatgrass case in Fig. 3. Fig. 4 shows only the results of the last stage of the average annual model, and Fig. 5 shows only the last stage of the interannual spline model. In these examples, data values < 0 are set equal to 0. The sole data value rejected at approximately 1999.4 is replaced by the value predicted for that time by the average annual model for the respective time series.

1) Average Annual Models: Fig. 4 shows the refined average annual models for the time series from the three classes of vegetation shown in Fig. 2. Fig. 4(a) illustrates the year-to-year similarity in amplitude and phase (timing) between the average annual model and the observed data for stable agriculture typical for an actively cultivated and irrigated site.

Fig. 4(b), shows the results for montane shrubland data. In general, the overall amplitude of the model matches quite well the overall amplitude of the observed data. However, there are systematic phase differences for particular years. For example, in the later part of 1999, the actual timing of senescence is somewhat later than what the average annual model would indicate, and in the later part of 2000, the actual timing of senescence is clearly earlier than what the average annual cycle would indicate. In 1998, the onset of green-up appears to be somewhat later than usual, which is likely due to late snow cover in the high mountain elevations.

The average annual results for cheatgrass in Fig. 4(c), show the most anomalous behavior of our examples. Although some years seem to be reasonably represented by the average annual model, in general, there are strong and striking disparities. The relatively unpredictable nature of cheatgrass is due to the amplified response of the species to periods of above-average precipitation, which result in significantly higher green amplitude and a very peaked phenology in cheatgrass communities. Bradley and Mustard [40] show that this behavior provides a significant signature in the NDVI data, serving to identify the location of this species and aiding in land cover classification.

2) Interannual Model Results: Fig. 5 shows the fit of the interannual spline model to the observed data for the three vegetation classes.

The phenology of the stable agricultural site [Fig. 5(a)], shows a very little year-to-year difference in seasonal cycles due to the strict irrigation and cultivation scheduling practiced at such sites in the Lovelock and Fallon agricultural districts. Sites without externally imposed environmental controls, for example the montane shrubland data in Fig. 5(b), show more variability, with the cheatgrass data in Fig. 5(c) showing the strongest interannual variability. Clearly, the type of strong interannual variability typical of semiarid grasslands is best captured by the interannual spline model. For more stable vegetation classes, however, such as the agricultural example in the top panel of Fig. 5, the prior average annual model in Fig. 4(a) fits the observations almost as well.

Examples of statistics that we have found helpful in model design during pilot runs are shown in Table II, which summarizes the distribution of residuals from the final-stage interannual spline for each type of time series shown in Fig. 5. As shown in the first row of data in the table, the total number of samples for each time series is 310. Because of the asymmetric weighting of the observed data to fit the upper data envelope, the number of positive residuals [as defined by (4)] is typically 75%–50% of the number of negative residuals. The standard deviation of the positive residuals is typically 30% of

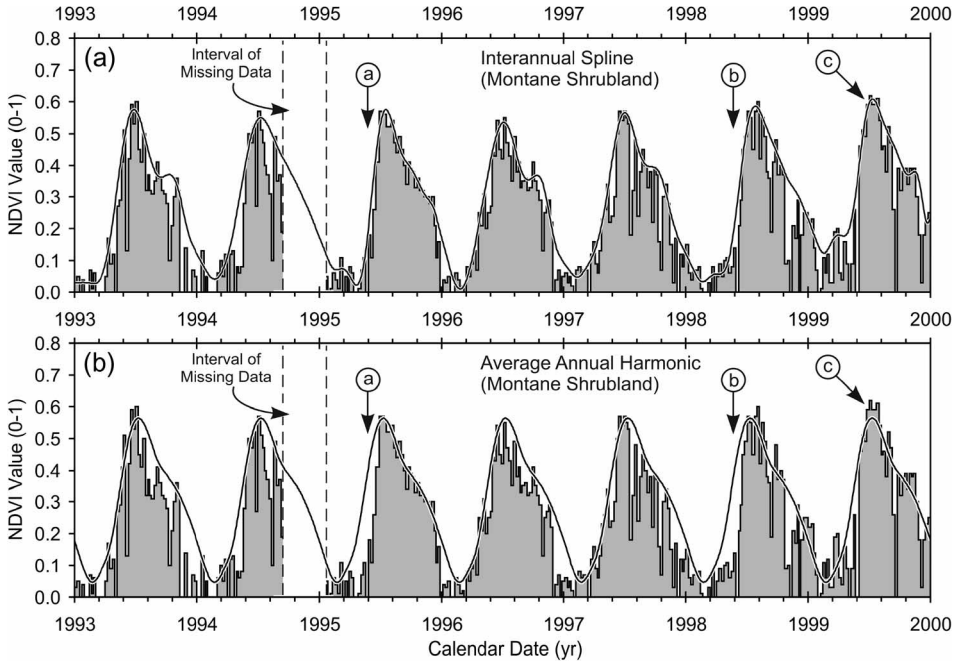

Fig. 6. Comparison of (a) the interannual spline model in this paper with (b) the average annual model of Hermance [21] for the same time series from a single 1×1 km montane shrubland site (at $39°18'$N, $117°8'16''$W). A substantial data gap (from 1994.72 to 1995.05) is due to sensor failure, which is denoted by the dashed blanked area. (a) Interannual model, using 14th-order annual splines. (b) Average annual model, using a 10th-order nonclassical harmonic series superposed on a zeroth-order polynomial (mean value).

the standard deviation of the negative residuals. These results serve as "rules-of-thumb" for selecting control parameters for areal studies that have a range of phenologies among plant communities. Attempting to fit the upper data envelope any more tightly on a global basis might lead to instabilities in fitting some of the more erratically behaved local time series. Note that, as expected, the statistics of the weighted residuals toward the bottom of the table have values that are much closer to each other, suggesting that the weighted residuals have a more normal distribution.

E. Illustrating the "Gap-Filling" Ability of the Algorithm

Hermance [21] argues that a significant feature of the nonclassical Fourier series approach is that an average annual model can be computed from noncontiguous data from multiple years. These synthesized values can then be used to replace missing or rejected data values when computing the next-stage refined model. We illustrate this for the seven-year montane shrubland time series in Fig. 6 from 1993 to 2000. (The observed data are from a longer time series at this same site used by Bradley *et al.* [19].) This time interval contains a substantial data gap in NDVI values during the late 1994 when the AVHRR sensor on board NOAA-11 failed, causing a loss of data until NOAA-14 could be launched and become operational. Hermance [21] previously used this same montane shrubland data set to illustrate the application of the nonclassical Fourier series to reconstructing the average annual NDVI behavior during a seven-year time window containing the time of instrument failure.

Here, we extend that analysis to include the results of the interannual spline algorithm shown in Fig. 6(a). For comparison, we reproduce in Fig. 6(b) the average annual harmonic model of Hermance [21], who showed that the nonclassical composite harmonic modeling algorithm smoothly interpolates estimated values throughout the end-of-1994 data gap. The average annual fit in panel (b) reasonably tracks the onset of green-up in 1993, 1994, 1996, 1997, and 1999. However, the interannual spline model in panel (a) is much better in tracking green-up for those years that have a significant departure from the mean green-up time, such as those flagged by the symbol "a" in 1995 and the symbol "b" in 1998. Late spring temperatures were significantly cooler during these two years in the west-central Great Basin, leading to late loss of snow cover and later-than-normal green-up. Moreover, the interannual spline is better at tracking some of the interannual variations in peak NDVI amplitude, such as those flagged by "c" in both panels of Fig. 6. In addition to the montane shrubland example presented here, examples of how the algorithm deals with such extended data gaps in time series from sagebrush sites and cheatgrass sites are presented by Bradley *et al.* [19].

V. Discussion and Conclusion

The basic premise of this study is that by having better tools to identify, monitor, and discriminate among plant communities, one will be better able to assess land cover responses to forcing from environmental and climate factors. We are particularly interested in increasing the time resolution of procedures for extracting NDVI signals from multiyear time series, with a view toward using these phenological responses to better identify and classify land cover and to monitor land cover change on local and regional scales. The interannual spline algorithm appears to be computationally robust and stable and adaptive in tracking the phenology of diverse vegetation communities with a minimum amount of user intervention.

When implementing such a computational scheme for a large-area study, it is advisable to run a number of pilot examples that cover the range of possible vegetation responses to be expected to best determine the set of tradeoffs among sharpness of response, damping of roughness, interannual versus intra-annual variability, and, of course, computation time. In other words, we do not recommend that the procedures described here be used on any and all data sets without supervision and prior testing. In fact, supervision—which involves the close inspection of the quality of how well the model tracks the particular attributes of a specific plant species under investigation—will be an effective way to "tune" the model in adapting to particular classes of vegetation types. Although to some degree the algorithm can "self-teach" itself through sequential recursions, this becomes computationally intensive and time consuming as well, although at this point we have not felt the computational efficiency of the algorithm, namely computer time, to be an issue for the local and regional applications that we have in mind. However, without a doubt, the present algorithm will be substantially slower than annual harmonic series analysis or the simplest adaptations of the asymmetric Gaussian functions, wavelets, and asymmetric logistic functions. We have been willing to forego computation speed in return for increasing the level of detail that we can achieve in characterizing phenological signatures.

One of the key objectives of our effort was to experiment with an algorithm whereby one size fits all, which means that a set of model control parameters can be assigned for a specific investigation—a random array of vegetation types—that will allow the model computations to adapt to a variety of different responses: differences from year-to-year for specific series and differences between series from different sites. Figs. 4 and 5 show the products of such an approach.

Overall, the interannual spline model adapts to tracking the fine structure of the phenology of the three diverse data sets quite well. Many of the key phenological attributes in Table I are readily identified visually in the NDVI signals of Fig. 5. Bradley *et al.* [19] use this interannual spline curve fit procedure to determine a subset of these metrics using the date-of-onset-of-greenness and date-of-maximum-NDVI to study land cover in the Great Basin.

Certain plant communities in our study area tend to have a strong persistent periodic seasonal component. Other vegetation communities have a more variable phenology. Even for the strongly dominant annually periodic montane shrubland data, there is a subtle year-to-year variation in the exact timing of green-up that appears to be largely driven by the disappearance of snow cover at the higher elevations. Other plant communities have pronounced impulsive aperiodic transient behaviors. The response of the invasive grassland species, cheatgrass, is an extreme example of variable phenology that is apparent not only in its strong interannual variability, but also in the rapid fluctuations that can occur in any given year. In summary, the interannual spline algorithm seems to be able to track the behavior of a variety of phenologies quite well, readily adapting to a range periodic to aperiodic behaviors that have characteristic time scales from a few weeks to years.

REFERENCES

[1] S. Azzali and M. Menenti, "Mapping vegetation–soil–climate complexes in southern Africa using temporal Fourier analysis of NOAA-AVHRR NDVI data," *Int. J. Remote Sens.*, vol. 21, no. 5, pp. 973–996, Mar. 2000.

[2] G. J. Roerink, M. Menenti, and W. Verhoef, "Reconstructing cloud-free NDVI composites using Fourier analysis of time series," *Int. J. Remote Sens.*, vol. 21, no. 9, pp. 1911–1917, Jun. 2000.

[3] A. Moody and D. M. Johnson, "Land-surface phenologies from AVHRR using the discrete Fourier transform," *Remote Sens. Environ.*, vol. 75, no. 3, pp. 305–323, Mar. 2001.

[4] M. E. Jakubauskas, D. R. Legates, and J. H. Kastens, "Harmonic analysis of time-series AVHRR NDVI data," *Photogramm. Eng. Remote Sens.*, vol. 67, no. 4, pp. 461–470, 2001.

[5] M. E. Jakubauskas, D. R. Legates, and J. H. Kastens, "Crop identification using harmonic analysis of time-series AVHRR NDVI data," *Comput. Electron. Agric.*, vol. 37, no. 1, pp. 127–139, Dec. 2002.

[6] M. E. Jakubauskas, D. L. Peterson, J. H. Kastens, and D. R. Legates, "Time series remote sensing of landscape–vegetation interactions in the southern Great Plains," *Photogramm. Eng. Remote Sens.*, vol. 68, no. 10, pp. 1021–1030, 2002.

[7] P. Jonsson and L. Eklundh, "Seasonality extraction and noise removal by function fitting to time-series of satellite sensor data," *IEEE Trans. Geosci. Remote Sens.*, vol. 40, no. 8, pp. 1824–1832, Aug. 2002.

[8] P. Jonsson and L. Eklundh, "TIMESAT—A program for analyzing time-series of satellite sensor data," *Comput. Geosci.*, vol. 30, no. 8, pp. 833–845, 2004.

[9] J. H. Kastens, M. E. Jakubauskas, and D. E. Lerner, "Using temporal averaging to decouple annual and nonannual information in AVHRR NDVI time series," *IEEE Trans. Geosci. Remote Sens.*, vol. 41, no. 11, pp. 2590–2594, Nov. 2003.

[10] X. Y. Zhang, M. A. Friedl, C. B. Schaaf, A. H. Strahler, J. C. F. Hodges, F. Gao, B. C. Reed, and A. Huete, "Monitoring vegetation phenology using MODIS," *Remote Sens. Environ.*, vol. 84, no. 3, pp. 471–475, Mar. 2003.

[11] J. Chen, P. Jonsson, M. Tamura, Z. Gu, B. Matsushita, and L. Eklundh, "A simple method for reconstructing a high-quality NDVI time-series data set based on the Savitzky–Golay filter," *Remote Sens. Environ.*, vol. 91, no. 3/4, pp. 332–344, 2004.

[12] S. Sarkar and M. Kafatos, "Interannual variability of vegetation over the Indian sub-continent and its relation to the different meteorological parameters," *Remote Sens. Environ.*, vol. 90, no. 2, pp. 268–280, 2004.

[13] R. Geerken, B. Zaitchik, and J. P. Evans, "Classifying rangeland vegetation type and coverage from NDVI time series using Fourier filtered cycle similarity," *Int. J. Remote Sens.*, vol. 26, no. 24, pp. 5535–5554, Dec. 2005.

[14] P. S. A. Beck, C. Atzberger, K. A. Høgda, B. Johansen, and A. K. Skidmore, "Improved monitoring of vegetation dynamics at very high latitudes: A new method using MODIS NDVI," *Remote Sens. Environ.*, vol. 100, no. 3, pp. 321–334, Feb. 2006.

[15] J. I. Fisher, J. F. Mustard, and M. A. Vadeboncoeur, "Green leaf phenology at Landsat resolution: Scaling from the field to the satellite," *Remote Sens. Environ.*, vol. 100, no. 2, pp. 265–279, Jan. 2006.

[16] C. J. Tucker, "Red and photographic infrared linear combinations for monitoring vegetation," *Remote Sens. Environ.*, vol. 8, no. 2, pp. 127–150, 1979.

[17] C. J. Tucker and P. J. Sellers, "Satellite remote sensing of primary production," *Int. J. Remote Sens.*, vol. 7, no. 11, pp. 1395–1416, 1986.

[18] R. B. Myneni, C. J. Tucker, G. Asrar, and C. D. Keeling, "Interannual variations in satellite-sensed vegetation index data from 1981 to 1991," *J. Geophys. Res.*, vol. 103, no. D6, pp. 6145–6160, 1998.

[19] B. A. Bradley, R. W. Jacob, J. F. Hermance, and J. F. Mustard, "A curve fitting procedure to derive inter-annual phenologies from time series of noisy satellite NDVI data," *Remote Sens. Environ.*, vol. 106, no. 2, pp. 137–145, Jan. 2007.

[20] Z. T. Li and M. Kafatos, "Interannual variability of vegetation in the United States and its relation to El Nino/Southern Oscillation," *Remote Sens. Environ.*, vol. 71, no. 3, pp. 239–247, Mar. 2000.

[21] J. F. Hermance, "Stabilizing high-order, non-classical harmonic analysis of NDVI Data for average annual models by damping model roughness," *Int. J. Remote Sens.*, vol. 28, no. 12, pp. 2801–2819, Jan. 2007.

[22] J. W. Rouse, R. H. Haas, J. A. Schnell, and D. W. Deering, "Monitoring the vernal advancement and retrogradation (green wave effect) of natural vegetation," in NASA/GSFC Type II Progress Report," Greenbelt, MD, 1973.

[23] B. C. Reed, J. F. Brown, D. VanderZee, T. R. Loveland, J. W. Merchant, and D. O. Ohlen, "Measuring phenological variability from satellite imagery," *J. Veg. Sci.*, vol. 5, no. 5, pp. 703–714, 1994.

[24] M. Menenti, L. Azzali, W. Verhoef, and R. Van Swol, "Mapping agroecological zones and time lag in vegetation growth by means of Fourier analysis of time series of NDVI images," *Adv. Space Res.*, vol. 13, no. 5, pp. 233–237, May 1993.
[25] P. J. Sellers, C. J. Tucker, G. J. Collatz, S. O. Los, C. O. Justice, D. A. Dazlich, and D. A. Randall, "A global 1° by 1° data set for climate studies—Part 2: The generation of global fields of terrestrial biophysical parameters from the NDVI," *Int. J. Remote Sens.*, vol. 15, no. 17, pp. 3519–3545, 1994.
[26] L. Olsson and L. Eklundh, "Fourier series for analysis of temporal sequences of satellite sensor imagery," *Int. J. Remote Sens.*, vol. 15, no. 18, pp. 3735–3741, 1994.
[27] L. Andres, W. A. Salas, and D. Skole, "Fourier analysis of multi-temporal AVHRR data applied to a land cover classification," *Int. J. Remote Sens.*, vol. 15, no. 5, pp. 1115–1121, 1994.
[28] J. P. Evans and R. Geerken, "Classifying rangeland vegetation type and coverage using a Fourier component based similarity measure," *Remote Sens. Environ.*, vol. 105, no. 1, pp. 1–8, 2006.
[29] H. Wagenseil and C. Samimi, "Assessing spatio-temporal variations in plant phenology using Fourier analysis on NDVI time series: Results from a dry savannah environment in Namibia," *Int. J. Remote Sens.*, vol. 27, no. 15/16, pp. 3455–3471, 2006.
[30] R. S. Lunetta, J. F. Knight, J. Ediriwickrema, J. G. Lyon, and L. D. Worthy, "Land-cover change detection using multi-temporal MODIS NDVI data," *Remote Sens. Environ.*, vol. 105, no. 2, pp. 142–154, Nov. 2006.
[31] G. E. Forsythe, M. A. Malcolm, and C. B. Moler, *Computer Methods for Mathematical Computations*. Englewood Cliffs, NJ: Prentice-Hall, 1977.
[32] P. Lancaster and K. Salkauskas, *Curve and Surface Fitting; An Introduction*. New York: Academic, 1986.
[33] S. Sarkar, L. Chiu, M. Kafatos, and R. Singh, "Sensitivity of rainfall on land cover change over South East Asia: Some observational results," *Adv. Space Res.*, vol. 39, no. 1, pp. 73–78, 2007.
[34] R. Esch, "Functional approximation," in *Handbook of Applied Mathematics*, K. Pearson, Ed. New York: Van Nostrand Reinhold, 1974, ch. 17, pp. 942–1001.
[35] EROS. (2005). *The Conterminous United States and Alaska Weekly and Biweekly AVHRR Composites*. [Online]. Available: http://lpdaac.usgs.gov/1km/paper.asp
[36] J. C. Eidenshink, "The 1990 conterminous U.S. AVHRR data set," *Photogramm. Eng. Remote Sens.*, vol. 58, no. 6, pp. 809–813, 1992.
[37] J. C. Eidenshink and J. L. Faundeen, "1-km AVHRR global land dataset: First stages in implementation," *Int. J. Remote Sens.*, vol. 15, no. 17, pp. 3443–3462, 1994.
[38] P. M. Teillet, N. E. Saleous, M. C. Hansen, J. C. Eidenshink, C. O. Justice, and J. R. G. Townshend, "An evaluation of the global 1-km AVHRR land dataset," *Int. J. Remote Sens.*, vol. 21, no. 10, pp. 1987–2021, Jul. 2000.
[39] M. E. Brown, J. Pinzon, and C. Tucker, "New vegetation index dataset available to monitor global change," *EOS Trans.*, vol. 85, no. 52, pp. 565–569, 2004.
[40] B. A. Bradley and J. F. Mustard, "Identifying land cover variability distinct from land cover change: Cheatgrass in the Great Basin," *Remote Sens. Environ.*, vol. 94, no. 2, pp. 204–213, 2005.

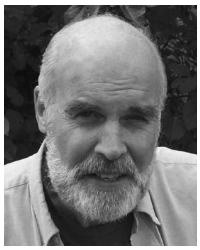

John F. Hermance received the Ph.D. degree in physics from the University of Toronto, Toronto, ON, Canada, in 1967.

From 1967 to 1968, he was a Research Associate with the Massachusetts Institute of Technology (MIT), Cambridge, participating in the National Aeronautics Space Administration (NASA)/MIT Apollo Applications Program and being responsible for designing and assessing the feasibility of various radio frequency "sounder" experiments during manned lunar landings. Since 1968, he has been with the faculty of the Department of Geological Sciences, Brown University, Providence, RI, where he is currently a Professor of geophysics and hydrology. He was a Visiting Faculty Fellow with the Phillips Petroleum Research Center, Bartlesville, OK, in 1974, and a Visiting Senior Research Associate with the Lamont-Doherty Geological Observatory from 1975 to 1976. He has directed numerous geophysical field projects in Iceland, the Azores, the Yukon, Canada, and throughout the U.S.

Prof. Hermance is a member of the American Geophysical Union, the Society of Exploration Geophysicists, the Association of Ground Water Scientists and Engineers/National Ground Water Association, and the Environmental and Engineering Geophysical Society.

Robert W. Jacob received the B.Sc. degree from Bucknell University in 1997 and the M.Sc. degree and the Ph.D. degree in geophysics and hydrology from Brown University, Providence, RI, in 2003 and 2006, respectively.

Prior to beginning his doctorate at Brown University in 2001, he was with Roy F. Weston, Inc., (currently Weston Solutions) for four years as an environmental/geophysical consultant. He currently has a postdoctoral research appointment with the Department of Geological Sciences, Brown University, continuing his dissertation work on remotely sensing unsaturated hydrologic processes. He has conducted multiple geophysical studies within archeological, planetary, and environmental research projects in Argentina and throughout the U.S. In addition to his research, he teaches geology classes at the Rhode Island School of Design.

Dr. Jacob is a member of the American Geophysical Union, the Society of Exploration Geophysics, the Environmental and Engineering Geophysics Society, Sigma Chi, and the Soil Science Society of America.

Bethany A. Bradley received the B.Sc. degree from Pomona College, Claremont, CA, in 2000 and the M.Sc. degree in geological sciences and the Ph.D. degree from Brown University, Providence, RI, in 2003 and 2006, respectively. Her Ph.D. work was the analysis of regional causes and impacts of land cover change and trends in the Great Basin of the U.S.

From 2000 to 2001, she was a Research Analyst at the National Aeronautics and Space Administration Goddard Space Flight Center. She is currently a Research Associate with the Woodrow Wilson School for Public and International Affairs, Princeton University, Princeton, NJ. Her principal research interests include how land cover responds to both natural changes such as weather fluctuations and anthropogenically driven changes such as land use or global climate change.

Dr. Bradley is a member of the American Geophysical Union, the Ecological Society of America, the Association of American Geographers, and the Great Basin Invasive Species and Remote Sensing Working Group.

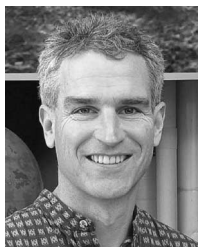

John F. Mustard received the Ph.D. degree from Brown University, Providence, RI, in 1990.

He was appointed to the research faculty of Brown University from 1991–1996. Since 1996, he has been with the faculty of the Department of Geological Sciences, Brown University, where he is currently a Professor of geological sciences and environmental studies. He has participated in numerous spacecraft missions including the Earth Observer 1 and several missions to Mars, including the European Mars Express and the National Aeronautics and Space Administration Mars Reconnaissance Orbiter. His research interests include the development of hyperspectral technologies for geologic and ecologic investigations.

Prof. Mustard is a member of the American Geophysical Union, the American Association for the Advancement of Science, and the American Society for Photogrammetry and Remote Sensing.